

Renormalization group study of electromagnetic interaction in multi-Dirac-node systems

Hiroki Isobe¹ and Naoto Nagaosa^{1,2}

¹*Department of Applied Physics, University of Tokyo, Tokyo 113-8656, Japan*

²*RIKEN Center for Emergent Matter Science, ASI, RIKEN, Wako, Saitama 351-0198, Japan*

(Dated: October 5, 2018)

We theoretically study the electromagnetic interaction in Dirac systems with N nodes by using the renormalization group, which is relevant to the quantum critical phenomena of topological phase transition ($N = 1$) and Weyl semimetals ($N = 4$ or $N = 12$). Compared with the previous work for $N = 1$ [H. Isobe and N. Nagaosa, *Phys. Rev. B* **86**, 165127 (2012)], we obtained the analytic solution for the large N limit, which differs qualitatively for the scaling of the speed of light c and that of electron v , i.e., v does not change while c is reduced to v . We also found a reasonably accurate approximate analytic solution for generic N , which well interpolates between $N = 1$ and large N limit, and it concludes that $c^2 v^N$ is almost unrenormalized. The temperature dependence of the physical properties, the dielectric constant, magnetic susceptibility, spectral function, DC conductivity, and mass gap are discussed based on these results.

PACS numbers: 73.43.Nq, 64.70.Tg, 71.10.-w

I. INTRODUCTION

Dirac fermions are spin 1/2 particles described by the basic equation of the relativistic quantum mechanics, the Dirac equation.¹ Since it is based on the special relativity, the Dirac equation is invariant under the Lorentz transformation. Dirac fermions are described by four-component spinors, and their components correspond to positive and negative energy and spin freedom. When the mass of a Dirac fermion is nonzero, the four-component representation is irreducible, but in the massless case, it becomes reducible to be a two-component representation. This two-component fermion is called a Weyl fermion. There exists the chiral symmetry for Weyl fermions, so they can be distinguished by the chirality. Right-handed or left-handed Weyl fermions cannot exist independently, thus the number of Weyl fermions is always even. This is the result of the fermion doubling theorem.²

The interaction between Dirac fermions and electromagnetic field is formulated in quantum electrodynamics (QED), and the exchange of photons mediates the interaction force. In QED, the speed of electron v and that of light c has the same value, and QED is the Lorentz-invariant theory. QED is also known as the most precise theory in physics.

The electronic states in solids are described by the Bloch wave functions, and according to the band theory, the equation equivalent to the Dirac equation may appear. One such example is graphene, a two-dimensional carbon sheet forming hexagonal lattice.³ The effective theory is described by the 2×2 Dirac Hamiltonian, and Dirac spectra appear at K and K' points in the Brillouin zone. Another example is bismuth, which exhibits a four-component massive Dirac fermion caused by spin-orbit interaction.⁴ Topological insulators also have Dirac spectrum on the surface.^{5,6} Although the bulk is insulating and gapped in topological insulators, the gap closes at the

quantum phase transition between topological and trivial insulators. The effective theory at the critical point is described by the 4×4 Dirac Hamiltonian for the systems with inversion symmetry, and the sign change of mass m corresponds to the phase transition. Namely, in this case the number of the Dirac fermion N is 1. This scenario is experimentally confirmed in $\text{BiTl}(\text{S}_{1-x}\text{Se}_x)_2$ by changing the concentration x .^{7,8} Pyrochlore iridates are predicted to be Weyl semimetals, where Weyl nodes are located on the Fermi surface. Band calculations indicate that there are $2N = 24$ (or $2N = 8$) Weyl nodes exist in pyrochlore iridates.^{9,10}

When a Dirac point is located on the Fermi level, the electron-electron interaction is not well screened, and becomes a long-range force. Thus, the effective model for Dirac fermion in solids has nearly equivalent form to QED. The renormalization group (RG) is used to deal with divergent integrals appearing in the perturbative treatment of the interaction. Here we should note one important difference from QED. In the band theory, the group velocity of electron v is expressed by the derivative of the energy dispersion in terms of the crystal momentum, but this v is far smaller than the speed of light in solid c . Therefore, the Lorentz invariance is broken in this model. The smallness of the factor v/c naturally leads to the choice of Coulomb gauge, where the scalar potential gives the instantaneous Coulomb interaction though the transverse part of the vector potential is often neglected.

The effects of electron-electron interaction on Dirac electrons are extensively studied.¹¹⁻¹⁴ RG analyses of Dirac electrons considering instantaneous Coulomb interaction in two and three dimensions¹¹⁻¹³ reveal the logarithmic divergence of v , while the coupling constant α is marginally irrelevant. In these analyses, c is not renormalized and stays constant. The divergence of v contradicts the assumption that the factor v/c is small. When the contribution from the vector potential is considered for 2D system, v saturates to c , and the Lorentz invari-

ance is recovered in the low-energy limit.¹⁴ The quantum critical behavior of Dirac electrons close to the superconducting transition is also studied.¹⁵ For 3D system, the previous study for $N = 1$ ¹⁶ reveals the renormalization of c in addition to v , and the recovery of Lorentz invariance in the low-energy limit. However, as mentioned above, there are cases where the number of Dirac nodes N takes several values in condensed matter systems, and it is important to extend the analysis to the generic N .

In this paper, we study the electromagnetic interaction in multinode Dirac and Weyl systems. Especially, in the limit of large N , we can obtain the analytic solution to RG equations. For generic N , we found a reasonably accurate approximate solution that interpolates the two limits, i.e., $N = 1$ and large N . By these results, we have revealed the global view of the RG flow in this problem and clarified the condition for neglecting the transverse channels of the electromagnetic interaction. We also made corrections of the previous study.¹⁶

II. MODEL

In this study we use the following Lagrangian:

$$\mathcal{L} = \bar{\psi}_a(\gamma^0 p_0 - v\boldsymbol{\gamma} \cdot \mathbf{p} - m)\psi_a + \frac{1}{2}(\varepsilon\mathbf{E}^2 - \frac{1}{\mu}\mathbf{B}^2) - e\bar{\psi}_a l_\nu^\mu \gamma^\nu \psi_a A_\mu. \quad (1)$$

Here ψ_a is a four-component Dirac spinor with a being the N node index. The matrix

$$l_\nu^\mu = \begin{pmatrix} 1 & & & \\ & v/c & & \\ & & v/c & \\ & & & v/c \end{pmatrix} \quad (2)$$

is introduced to describe the electromagnetic interaction in a system without Lorentz invariance. The metric used in the model is $(+ - - -)$. We mostly focus on the massless case ($m = 0$), which corresponds to a quantum critical point of topological insulators and Weyl semimetals. The RG effect on m is discussed later.

To accurately describe the topological insulator phase, the θ term is necessary; i.e., we should add $\theta\mathbf{E} \cdot \mathbf{B}$ ($\theta = \pm\pi$) to the action. The θ term is omitted in the model because this term can be transformed into the surface term and we do not consider the topological magnetoelectric effect in the present analysis. Actually, the RG analysis does not modify the θ term. It is natural since topological terms have discrete integer values, and we confirmed this fact from the following two methods: the perturbative calculation and the background field theory. In any case, the topological θ term does not alter the bulk properties.

If we consider massless Weyl nodes, the Lagrangian has the chiral symmetry, and a four-component Dirac spinor can be separated into two two-component Weyl spinors with opposite chiralities. Thus, the number of

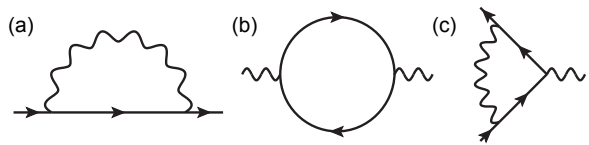


FIG. 1. Feynman diagrams at one-loop order: (a) self-energy, (b) polarization, (c) vertex.

Weyl nodes N_W are twice as large as that of Dirac nodes N , i.e., $N_W = 2N$. In the following analysis, we treat the model in the four-component notation. If necessary, we can use the projection operator $(1 \pm \gamma^5)/2$ to separate a massless Dirac fermion into two Weyl fermions with opposite chiralities.

The permittivity ε and the permeability μ determine the speed of light in material $c = c_{\text{vacuum}}/\sqrt{\varepsilon\mu}$, where $c_{\text{vacuum}} = 3 \times 10^8$ m/s is that in vacuum. c also sets the speed of electromagnetic interaction in material. The electric and magnetic fields are written as

$$\mathbf{E} = -\frac{1}{c} \frac{\partial \mathbf{A}}{\partial t} - \nabla A_0, \quad \mathbf{B} = \frac{1}{c} \nabla \times \mathbf{A}. \quad (3)$$

The electron propagator $G_0(p)$, the photon propagator $D_0^{\mu\nu}(q)$, and the vertex Γ_0^μ are given by

$$G_0(p) = \frac{i}{\gamma^0 p_0 + v\gamma^\alpha p_\alpha + i0}, \quad (4)$$

$$D_0^{\mu\nu}(q) = \frac{-ic^2 g^{\mu\nu}}{\varepsilon(q_0^2 - c^2 q_\alpha^2) + i0}, \quad (5)$$

$$\Gamma_0^\mu = -iel_\nu^\mu \gamma^\nu = \left(-ie\gamma^0, -ie\frac{v}{c}\gamma^\alpha\right). \quad (6)$$

We have used the Feynman gauge for the photon propagator. Physical quantities are independent of the gauge choice.

III. RENORMALIZATION GROUP ANALYSIS

We calculated the Feynman diagrams to one-loop order (Fig. 1) to derive the RG equations:

$$\kappa \frac{dv}{d\kappa} = -\frac{2g^2}{3\pi} \frac{c^2}{(c+v)^2} \left[1 + 2\left(\frac{v}{c}\right) + \left(\frac{v}{c}\right)^2 - 4\left(\frac{v}{c}\right)^3\right], \quad (7)$$

$$\kappa \frac{dc}{d\kappa} = \frac{Ng^2}{3\pi} \frac{c}{v} \left[1 - \left(\frac{v}{c}\right)^2\right], \quad (8)$$

$$\kappa \frac{dg^2}{d\kappa} = \frac{2Ng^4}{3\pi} \frac{1}{v}. \quad (9)$$

Here, κ denotes the momentum scale. The details of the calculation for $N = 1$ are described in the previous paper.¹⁶

A. Large N limit

We set a parameter λ , which measures the effect of a polarization bubble compared to the bare propagator, as

$$\lambda = N\alpha = \frac{Ng^2}{v}. \quad (10)$$

If we write the RG equations in terms of λ instead of g , we obtain

$$\frac{dv}{dl} = \frac{2\lambda}{3\pi N} \frac{c^2 v}{(c+v)^2} \left[1 + 2\left(\frac{v}{c}\right) + \left(\frac{v}{c}\right)^2 - 4\left(\frac{v}{c}\right)^3 \right], \quad (11)$$

$$\frac{dc}{dl} = -\frac{\lambda}{3\pi} c \left[1 - \left(\frac{v}{c}\right)^2 \right], \quad (12)$$

$$\frac{d\lambda}{dl} = -\frac{2\lambda^2}{3\pi} - \frac{2\lambda^2}{3\pi N} \left[1 + 2\left(\frac{v}{c}\right) + \left(\frac{v}{c}\right)^2 - 4\left(\frac{v}{c}\right)^3 \right]. \quad (13)$$

where we define $l = \ln(\kappa_0/\kappa)$. Terms proportional to $1/N$ vanish in the large N limit ($N \rightarrow \infty$), and the analytical solutions to the RG equations are easily obtained as

$$v(l) = v_0 \text{ (const.)}, \quad (14)$$

$$c(l) = \left[v_0^2 + (c_0^2 - v_0^2) \left(1 + \frac{2\lambda_0}{3\pi} l \right)^{-1} \right]^{1/2}, \quad (15)$$

$$\lambda(l) = \lambda_0 \left(1 + \frac{2\lambda_0}{3\pi} l \right)^{-1}. \quad (16)$$

From Eq. (15), we can confirm $c(l) \rightarrow v_0$ ($l \rightarrow \infty$), while v is not renormalized. This is in sharp contrast to the result obtained by neglecting the transverse electromagnetic field, where v diverges logarithmically. It means the recovery of the Lorentz invariance in the infrared (IR) limit.

B. Numerical solutions

The RG equations (7), (8), and (9) for generic N cannot be solved analytically without any approximations, so we first solve them numerically. The numerical solutions to the RG equations are shown in Figs. 2 and 3. We set the initial (bare) values of $v_0 = 0.001$ and $\varepsilon_0 = 10$ and consider a nonmagnetic material ($\mu_0 = 1$). In this case, $c_0 = 0.32$ and $\alpha_0 = 0.73$, where the dimensionless coupling constant α is defined by

$$\alpha = \frac{g^2}{v} = \frac{e^2}{(4\pi\varepsilon)v}. \quad (17)$$

We can find some important features from the result. First, the speed of electron v and that of light c coincide to be the common value $c_\infty = (c_0^2 v_0^N)^{1/(N+2)}$ in the IR limit. Second, the quantity $c^2 v^N$ is almost constant for all momentum scale. We make use of this fact for the

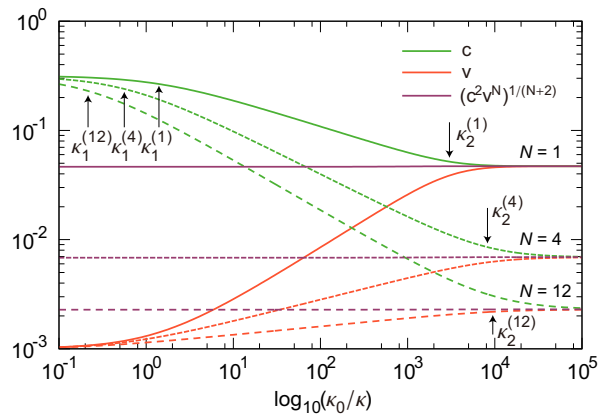


FIG. 2. (Color online) Numerical solutions to the RG equations for v and c . We set the initial values $v_0 = 0.001$ and $\varepsilon_0 = 10$. A nonmagnetic material ($\mu_0 = 1$) is considered, and in this case, $c_0 = 0.32$ and $\alpha_0 = 0.73$. We can observe that the quantities $(c^2 v^N)^{1/(N+2)}$ are almost constant for all momentum scale.

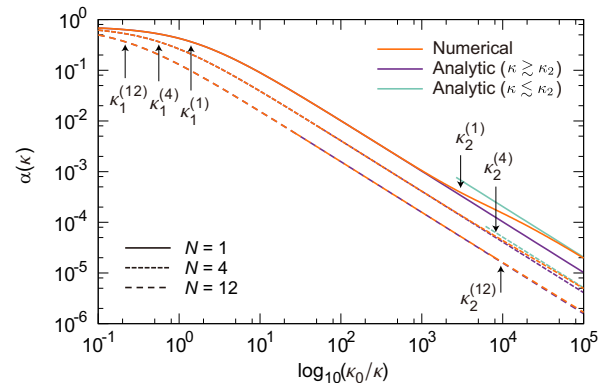


FIG. 3. (Color online) Numerical and analytic solutions to the RG equations for α . The analytic solutions for $\kappa \gtrsim \kappa_2$ and $\kappa \lesssim \kappa_2$ well explain the numerical solutions. As the number of species N increases, the difference between the analytic solutions for $\kappa \gtrsim \kappa_2$ and numerical solutions becomes smaller, and the analytic expression becomes more precise.

analytical solutions discussed below. Third, the dimensionless coupling constant α becomes smaller in the IR limit, which concludes the validity of the perturbative RG analysis. Therefore, the Lorentz invariance is recovered in the IR limit, and the system becomes equivalent to that of the conventional QED. Even if the Lorentz invariance is broken in the original Lagrangian, the RG analysis reveals that the system in the IR limit is the ideal laboratory to study QED.

C. Analytic solutions

As we saw in the numerical calculations, the quantity $c^2 v^N$ is almost constant independent of the momentum scale. From the RG equations, the scale dependence of

the quantity is

$$\begin{aligned} \frac{d(c^2 v^N)}{dl} &= 2c v^N \frac{dc}{dl} + N c^2 v^{N-1} \frac{dv}{dl} \\ &= \frac{2N g^2}{3\pi} c^2 v^{N-1} \frac{\beta^2 (1-\beta)^2}{(1+\beta)^2}, \end{aligned} \quad (18)$$

where $\beta = v/c$. If we define the function $f(\beta)$ as

$$f(\beta) = \frac{\beta^2 (1-\beta)^2}{(1+\beta)^2}, \quad (19)$$

and assume $v \leq c$, i.e. $0 \leq \beta \leq 1$, we obtain $0 \leq f(\beta) \leq 17 - 12\sqrt{2} \simeq 0.03$. The maximum value $g(\beta) \simeq 0.03$ is rarely observed in the scale of Fig. 2, and the right-hand side of Eq. (18) is always small for $0 < \beta < 1$. Therefore, the approximation

$$c^2 v^N = c_0^2 v_0^N \quad (20)$$

is satisfied for the entire energy scale.

The second approximation is

$$\frac{c}{c_0} = \frac{g}{g_0}. \quad (21)$$

It holds until c reaches the vicinity of the asymptotic value c_∞ . Actually, this approximation has a physical interpretation. Since $c = 1/\sqrt{\varepsilon\mu}$ and $g = e/\sqrt{4\pi\varepsilon}$, the equality means the permeability μ stays constant.

Using Eqs. (20), (21), we can analytically solve the RG equations (7), (8), and (9), and obtain

$$g^2(l) = g_0^2 \left(1 + \frac{2N+2}{3\pi} \alpha_0 l \right)^{-N/(N+1)}. \quad (22)$$

The other solutions follow by using the analytic expression of $g^2(l)$ as

$$v(l) = v_0 \left(1 + \frac{2N+2}{3\pi} \alpha_0 l \right)^{1/(N+1)}, \quad (23)$$

$$c(l) = c_0 \left(1 + \frac{2N+2}{3\pi} \alpha_0 l \right)^{-N/(2N+2)}, \quad (24)$$

$$\alpha(l) = \alpha_0 \left(1 + \frac{2N+2}{3\pi} \alpha_0 l \right)^{-1}. \quad (25)$$

These analytic expressions are valid for $\kappa \gtrsim \kappa_2$.

From the analytical solutions, we can identify the two momentum scales, κ_1 and κ_2 , as

$$\kappa_1^{(N)} = \exp \left[-\frac{3\pi}{(2N+2)\alpha_0} \right] \kappa_0, \quad (26a)$$

$$\kappa_2^{(N)} = \exp \left[-\frac{3\pi}{(2N+2)\alpha_0} \left[\left(\frac{c_0}{v_0} \right)^{(2N+2)/(N+2)} - 1 \right] \right] \kappa_0. \quad (26b)$$

κ_1 is determined by $\alpha(\kappa_1) = \alpha_0/2$ and κ_2 is the point where the analytically derived function $c(\kappa)$ coincides

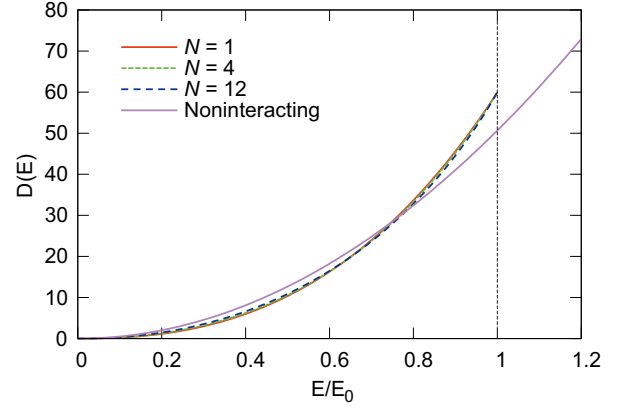


FIG. 4. (Color online) Density of states modified by the RG analysis. The DOS in the low-energy region is suppressed compared to the noninteracting one, due to the electron correlation effect. To compensate for the suppression, the DOS increases around $E/E_0 \gtrsim 0.8$. The effect of RG appears only below the cutoff energy E_0 .

with the asymptotic value c_∞ . Assuming $v_0/c_0 \ll 1$, $\kappa_2 \ll \kappa_1 < \kappa_0$ is satisfied. These characteristic momenta specify three scaling regions: (i) perturbative region $\kappa_1 \lesssim \kappa \lesssim \kappa_0$, where the deviation from the bare value is small and it can be treated perturbatively; (ii) nonrelativistic scaling region $\kappa_2 \lesssim \kappa \lesssim \kappa_1$, where the effect of RG becomes large, while the factor v/c is still small; and (iii) relativistic scaling region $\kappa \lesssim \kappa_2$, where $c(\kappa) \simeq v(\kappa)$ and the Lorentz invariance is recovered.

As to the dimensionless coupling constant α , its analytic expression can be obtained for region (iii), the relativistic scaling region. When we put $c = v = c_\infty$, the RG equation for α becomes

$$\frac{d\alpha}{dl} = -\frac{2N}{3\pi} \alpha^2, \quad (27)$$

and it can be solved analytically to obtain

$$\alpha(l) = \frac{3\pi}{2N} \frac{1}{l}. \quad (28)$$

Surprisingly, the coupling constant $\alpha(l)$ in region (iii) is independent of its bare value α_0 .

IV. PHYSICAL PROPERTIES

A. Density of states

The density of states (DOS) is an important quantity to determine the physical property of a material. From the RG analysis, the electron velocity $v(k)$ is not a constant, and the energy $E(k) = v(k)k$ is no longer linear in the momentum k below the cutoff. In general, the DOS of a system with energy $E(k)$ is determined as

$$D(E) = \int \frac{d^3k}{(2\pi)^3} \delta(E - E(k)) = \frac{1}{2\pi^2} \frac{k^2(E)}{E'(k(E))}, \quad (29)$$

where E' stands for dE/dk . The DOS is a function of energy, so all quantities should be expressed in terms of energy E .

The DOS for 3D noninteracting Dirac fermions is

$$D_0(E) = \frac{E^2}{2\pi^2 v_0^3}. \quad (30)$$

The RG effect on the DOS is calculated numerically and is compared with the noninteracting case in Fig. 4. Since $v(k)$ gets faster as the momentum scale goes to the IR region, the DOS is suppressed in the low-energy region. On the other hand, the DOS is increased for $0.8 \lesssim E/E_0 < 1$, where $E_0 = v_0 \kappa_0$ is the energy cutoff. This increase compensates for the suppression of the DOS in the low-energy region.

B. Electromagnetic properties

Here we consider the permittivity $\varepsilon(\kappa)$ and the permeability $\mu(\kappa)$. The scale dependence of the permittivity $\varepsilon(\kappa)$ is determined from that of g^2 . We consider that the scale dependence of g^2 emerges only from ε and that the bare electric charge e stays constant. The permeability is obtained by $\mu = 1/(\varepsilon c^2)$. The numerical solutions for ε and μ are shown in Fig. 5. For $\kappa \gtrsim \kappa_2$, the analytic solution to ε is easily obtained from Eq. (22) as

$$\varepsilon(l) = \varepsilon_0 \left(1 + \frac{2N+2}{3\pi} \alpha_0 l \right)^{N/(N+1)}. \quad (31)$$

From Fig. 5, we find that the characteristic momentum scales for ε and μ are different. The momentum scale κ is related to the temperature scale by $T \simeq v(\kappa)\kappa$; therefore, the permittivity $\varepsilon(\kappa)$ logarithmically increases below $T_1 = v(\kappa_1)\kappa_1$ and the permeability decreases below $T_2 = v(\kappa_2)\kappa_2$. This contrasting behavior helps us to experimentally determine the two characteristic scales. In the zero temperature limit, the permeability $\mu = 1 + 4\pi\chi$ (χ : magnetic susceptibility) goes to zero; i.e., the system shows the perfect diamagnetism with $\chi = 1/(4\pi)$.

C. Spectral function

The spectral function is obtained as the imaginary part of the electron Green's function, so we should carefully select the gauge. To calculate the spectral function, we adopt the ‘‘physical gauge,’’ i.e., Coulomb gauge. The photon propagator in the Coulomb gauge $D_C^{\mu\nu}(k)$ is given by¹⁷

$$D_C^{\mu\nu}(k) = \frac{c^2}{\varepsilon} \begin{pmatrix} \frac{1}{k^2} & 0 \\ 0 & -\frac{g^{\alpha\beta}}{k^2} - \frac{1}{k^2} \frac{k^\alpha k^\beta}{k^2} \end{pmatrix}. \quad (32)$$

From the Callan-Symanzik equation, the electron Green's function $G(\mathbf{k}, \omega)$ is obtained as the product of

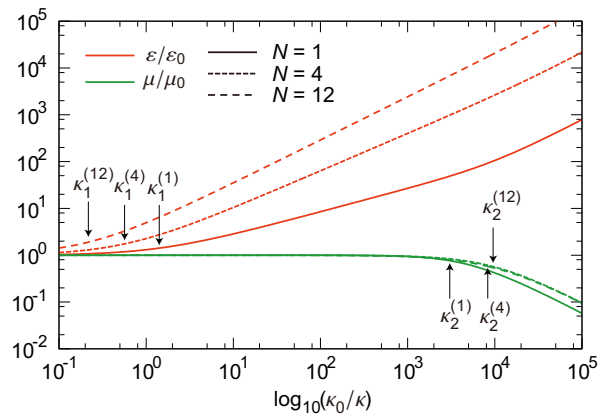


FIG. 5. (Color online) Numerical solutions to the RG equations for the permittivity ε and the permeability μ . The characteristic momentum scales for ε and μ are κ_1 and κ_2 , respectively.

the bare electron propagator, the electron field renormalization γ_2 , and the perturbative correction \mathcal{G} :

$$G(\mathbf{k}, \omega) = \frac{\mathcal{G}(\alpha(\kappa))}{\omega^2 - v^2(\kappa)\mathbf{k}^2} \exp \left[2 \int_{\Lambda}^k d \ln \left(\frac{k'}{\Lambda} \right) \gamma_2(\alpha) \right]. \quad (33)$$

k in this equation should be regarded as a magnitude of a spacelike vector, i.e., $k = \sqrt{v^2 \mathbf{k}^2 - \omega^2}$. The field renormalization γ_2 in the Coulomb gauge is given by¹⁶

$$\gamma_2(v, c, \alpha; \kappa) = \frac{\alpha}{\pi} \frac{v^3}{c(c+v)^2}. \quad (34)$$

In region (i), the field renormalization γ_2 is so small with the factor $(v/c)^3$ that the correction of the Green's function is negligible. On the other hand, the κ dependence of γ_2 in region (ii) is too complicated to calculate the Green's function. Hence, we concentrate on the analysis for region (iii), where simple analytic expressions exist.

From Eq. (28), $\gamma_2(k)$ is obtained as

$$\gamma_2(k) = \frac{\alpha(k)}{4\pi} = \frac{3}{8N} \left[\ln \left(\frac{\Lambda}{k} \right) \right]^{-1}. \quad (35)$$

The perturbative correction \mathcal{G} in region (iii) is small since the running coupling constant becomes small in this region,¹⁶ so we put $\mathcal{G} = 1$. Then we obtain the electron Green's function

$$G(\mathbf{k}, \omega) = \frac{1}{\omega^2 - c_\infty^2 \mathbf{k}^2} \left[\frac{1}{2} \ln \left(\frac{\Lambda^2}{c_\infty^2 \mathbf{k}^2 - \omega^2} \right) \right]^{-3/(4N)}. \quad (36)$$

The electron spectral function is obtained by the imaginary part of the Green's function $-\text{Im}G(\mathbf{k}, \omega + i0)$. It has finite value for $|\omega| \geq c_\infty |\mathbf{k}|$; otherwise, $-\text{Im}G(\mathbf{k}, \omega) = 0$. The spectral function in region (iii) has the approximate

form

$$\begin{aligned}
& -\text{Im}G(\mathbf{k}, \omega) \\
& \sim a\delta(\omega^2 - c_\infty^2 \mathbf{k}^2) \\
& + \frac{1}{\omega^2 - c_\infty^2 \mathbf{k}^2} \frac{3\pi}{8N} \left[\frac{1}{2} \ln \left| \frac{\Lambda^2}{c_\infty^2 \mathbf{k}^2 - \omega^2} \right| \right]^{-1-3/(4N)} \\
& \times \theta(\omega^2 - c_\infty^2 \mathbf{k}^2), \tag{37}
\end{aligned}$$

where the constant a is determined by the sum rule. The δ function peak with finite a indicates a Fermi liquid state, which is different from the (2+1)D analysis.¹⁴ The continuum state for $|\omega| > c_\infty k$ is emerged from the electron-electron interaction.

D. Electric conductivity

In this section, we calculate the electric conductivity for $\omega \ll T$ from the quantum Boltzmann equation (QBE) with the leading log approximation. Calculations are performed by following previous studies.^{12,13,18,19} The QBE in the external field \mathbf{F} is

$$\left[\frac{\partial}{\partial t} + \mathbf{F} \cdot \frac{\partial}{\partial \mathbf{k}} \right] f_{\lambda a}(\mathbf{k}, t) = -w[f_{\lambda a}(\mathbf{k}, t)], \tag{38}$$

where $f_{\lambda a}(\mathbf{k}, t)$ is a distribution function of particles and holes ($\lambda = \pm$), with a being a node index, and $w[f_{\lambda a}(\mathbf{k}, t)]$ represents the scattering rate due to the electron-electron interaction.

We assume that the external electric force $\mathbf{F} = e\mathbf{E}$ is weak, and that the deviation of the distribution function from the equilibrium $f_{\lambda a}^0(k) = (1 + e^{\beta\lambda vk})^{-1}$ is small, so that we consider the linear response in \mathbf{E} :

$$\begin{aligned}
f_{\lambda a}(\mathbf{k}, \omega) &= 2\pi\delta(\omega) f_{\lambda a}^0(k) \\
& + \lambda \frac{\mathbf{k} \cdot e\mathbf{E}(\omega)}{k} f_{\lambda a}^0(k) [1 - f_{\lambda a}^0(k)] g(k, \omega). \tag{39}
\end{aligned}$$

For $\omega \ll T$, the contribution from the particle-hole pair to the current density $\mathbf{j}(\omega)$ can be neglected, thus

$$\mathbf{j}(\omega) = ev \sum_{\lambda a} \int_{\mathbf{k}} \frac{\lambda \mathbf{k}}{k} f_{\lambda a}(\mathbf{k}, \omega). \tag{40}$$

Therefore, the electric conductivity $\sigma(\omega)$ is given by using the function $g(k, \omega)$ as

$$\sigma(\omega) = \frac{\mathbf{j}(\omega)}{E(\omega)} = e^2 v \sum_{\lambda a} \int_{\mathbf{k}} \frac{k_x^2}{k^2} f_{\lambda a}^0(k) [1 - f_{\lambda a}^0(k)] g(k, \omega). \tag{41}$$

We should determine $g(k, \omega)$ to obtain the electric conductivity. In equilibrium, the scattering rate $w[f^0] = 0$, so when we expand the scattering rate in terms of $g(k, \omega)$, the zeroth-order term vanishes, and we can write

$$w[f_{\lambda a}(\mathbf{k}, \omega)] = e\mathbf{E}(\omega) \cdot \mathcal{C}[\lambda g(k, \omega)\hat{\mathbf{k}}] + O(g^2), \tag{42}$$

where $\hat{\mathbf{k}} = \mathbf{k}/k$, and \mathcal{C} is called the collision operator. By using the collision operator, the QBE becomes

$$[i\omega g_a(k, \omega) + \beta v] \lambda \hat{\mathbf{k}} f_{\lambda a}^0(k) [1 - f_{\lambda a}^0(k)] = \mathcal{C}[\lambda \hat{\mathbf{k}} g(k, \omega)]. \tag{43}$$

To solve this equation, it is convenient to use a variational method. The variational functional $\mathcal{Q}[g]$ is given by

$$\begin{aligned}
\mathcal{Q}[g] &= \sum_a \int_{\mathbf{k}} \left[i\omega \frac{g^2(k, \omega)}{2} + \beta v g(k, \omega) \right] f_{\lambda a}^0(k) [1 - f_{\lambda a}^0(k)] \\
& - \frac{1}{2} \sum_a \int_{\mathbf{k}} \lambda \hat{\mathbf{k}} g(k, \omega) \mathcal{C}[\lambda \hat{\mathbf{k}} g(k, \omega)], \tag{44}
\end{aligned}$$

and the stationary point

$$\frac{\delta \mathcal{Q}[g]}{\delta g} = 0 \tag{45}$$

gives the solution $g(k, \omega)$.

When we assume the form $g(k, \omega) = k\xi(\omega)$, according to Fritz *et al.*¹⁹, we obtain the variational functional $\mathcal{Q}[k\xi(\omega)]$ as

$$\begin{aligned}
\mathcal{Q}[k\xi(\omega)] &= \frac{1}{4\pi^2} \frac{1}{(\beta v)^5} \left\{ i\omega \frac{7\pi^4}{30} [\xi(\omega)]^2 + 9(\beta v)^2 \zeta(3) \xi(\omega) \right\} \\
& - \frac{1}{2} \frac{2\pi N}{9\beta^6 v^5} (\alpha^2 \ln \alpha^{-1}) F\left(\frac{v}{c}\right) [\xi(\omega)]^2, \tag{46}
\end{aligned}$$

with the relativistic correction

$$F(x) = 1 + \frac{1}{4} \left[3 - x^2 - \frac{(1 - x^2)(3 + x^2)}{x} \tanh^{-1} x \right]. \tag{47}$$

The function $F(v/c)$ can be regarded as the relativistic correction, and it cannot be obtained from the previous nonrelativistic analyses. In the nonrelativistic limit ($v/c \rightarrow 0$), we have $F(v/c) = 1$, and it monotonically increases to $F(v/c) = 3/2$ ($v/c \rightarrow 1$).

Now we can determine $\xi(\omega)$ by the functional derivative as

$$\xi(\omega) = \frac{81\zeta(3)}{4\pi^3} \beta^3 v^2 \left[2N(\alpha^2 \ln \alpha^{-1}) F\left(\frac{v}{c}\right) - \frac{21\pi}{20} i\beta\omega \right]^{-1}, \tag{48}$$

and the electric conductivity is

$$\begin{aligned}
\sigma^{(N)}(\omega, T) &= 2N \frac{e^2}{h^2} \left(\frac{k_B T}{\hbar v} \right) \frac{243[\zeta(3)]^2}{4\pi^4} \\
& \times \left[2N(\alpha^2 \ln \alpha^{-1}) F\left(\frac{v}{c}\right) - \frac{21\pi}{20} i\beta\omega \right]^{-1}. \tag{49}
\end{aligned}$$

We recovered k_B and \hbar in the last line of the equation. Especially, the DC conductivity is

$$\sigma_{\text{DC}}^{(N)}(T) = \frac{e^2}{h} \frac{k_B T}{\hbar v} \frac{0.90}{\alpha^2 \ln \alpha^{-1} F(v/c)}, \tag{50}$$

as shown in Fig. 6.

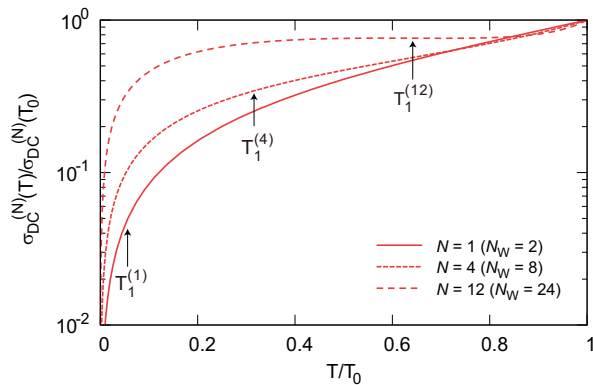


FIG. 6. (Color online) DC conductivity $\sigma_{\text{DC}}^{(N)}(T)$.

E. Energy gap

Finally, let us consider the RG effect on the mass parameter m . The mass m describes the critical behavior of the gap, and $m = 0$ at the critical point. For particular materials with Dirac nodes, the bare mass m_0 is tunable, depending on the concentration x or by pressure P .^{7,8}

The RG equation for mass $m(\kappa)$ is obtained from the electron self-energy as

$$\kappa \frac{dm}{d\kappa} = -\frac{3\alpha}{2\pi} m, \quad (51)$$

and its analytic solution for $\kappa \gtrsim \kappa_2$ is

$$m(\kappa) = m(\Lambda) \left[1 + \frac{2N+2}{3\pi} \alpha_0 \ln \left(\frac{\Lambda}{\kappa} \right) \right]^{9/(4N+4)}. \quad (52)$$

When we neglect the weak singularity of $\ln \ln m_0$, the solution to Eq. (52) becomes

$$m = m_0 \left[1 + \frac{2N+2}{3\pi} \alpha_0 \ln \left(\frac{\Lambda}{m_0} \right) \right]^{9/(4N+4)}. \quad (53)$$

V. DISCUSSIONS AND SUMMARY

Now we discuss the relevance of the present results to the real systems.

First, for a topological insulator ($N = 1$), the velocity v_0 is estimated at $v_0 \simeq 10^6$ m/s from the ARPES measurement of the energy dispersion⁷; hence, $c_{\text{vacuum}}/v_0 \simeq 300$. As for the dielectric constant ϵ , we take the typical value $\epsilon_0 \simeq 10^2$ of BiSb alloys.²⁰ Since $c_0 = c_{\text{vacuum}}/\sqrt{\epsilon_0}$, $c_0/v_0 \simeq 30$ and $\alpha_0 = (1/137)/(\epsilon v) \simeq 0.022$ are obtained. These values give the estimates for $\kappa_1 \simeq 10^{-47} \kappa_0$ and $\kappa_2 \ll \kappa_1$.

For the pyrochlore iridate $\text{Y}_2\text{Ir}_2\text{O}_7$ with $2N = 24$, the velocity and the dielectric constant may be estimated as $v_0 \simeq 10^6$ m/s and $\epsilon_0 \simeq 10$.¹³ In this case $c_0/v_0 \simeq 95$ and $\alpha_0 \simeq 0.22$, so we obtain $\kappa_1 \simeq 0.2\kappa_0$, and κ_2 is extremely small. The value $\kappa_1 \simeq 0.2\kappa_0$ would be physically accessible.

To experimentally observe the RG effects, we have to search materials with reasonably large κ_1 and κ_2 . A larger coupling constant α_0 is necessary to obtain larger κ_1 , and this can be realized if both of the dielectric constant ϵ_0 and the Fermi velocity v are small. In addition to large α_0 , small c_0/v_0 is required to make κ_2 larger. There seem to be two approaches: (a) small c_0 and (b) large v_0 . In case (a), a large dielectric constant ϵ_0 leads to the small coupling constant α_0 (assuming $\mu_0 = 1$), so it cannot be a solution. In case (b), a large v_0 also brings a small α_0 . The only way out is the small ratio of c_0/v_0 . Unfortunately, it would be difficult to observe the relativistic scaling behavior at the experimentally accessible temperature in the materials at hand.

This estimation gives a justification for the nonrelativistic approximation. Physically accessible κ_1 is easily obtained by choosing appropriate v_0 and ϵ_0 , but it would be difficult to access κ_2 unless $c_0 \approx v_0$. It means that the nonrelativistic approximation in the RG analysis is adequate in ordinary situations. However, if $c_0 \approx v_0$ is accomplished with $\epsilon_0 \sim 1$ and $\mu_0 \gg 1$, we might reach κ_2 , i.e., the relativistic scaling region.

In summary, we have studied the electromagnetic interaction in (3+1)D multi-node (N) Dirac systems by using RG analysis. The RG equations for the speed of light c , that of electron v , and the coupling constant α are derived for generic N . We solved the RG equations to obtain the analytic expressions for the large N limit and the reasonably accurate analytic solutions for generic N systems. We also discussed the physical quantities based on the RG analysis, which facilitates the observation of the scale-dependent behavior.

ACKNOWLEDGMENTS

We acknowledge fruitful discussions with S. Nakosai. This work is supported by Grant-in-Aid for Scientific Research (Grant No. 24224009) from the Ministry of Education, Culture, Sports, Science and Technology of Japan, Strategic International Cooperative Program (Joint Research Type) from Japan Science and Technology Agency, and Funding Program for World-Leading Innovative RD on Science and Technology (FIRST Program).

¹ For a description of the Dirac equation and QED, see for example M. E. Peskin and D. V. Schroeder, *An Introduction*

to Quantum Field Theory (Westview Press, 1995);

- P. Ramond, *Field Theory: A Modern Primer*, 2nd ed. (Addison-Wesley, 1990).
- ² H. Nielsen and M. Ninomiya, *Phys. Lett. B* **130**, 389 (1983).
 - ³ A. H. Castro Neto, F. Guinea, N. M. R. Peres, K. S. Novoselov, and A. K. Geim, *Rev. Mod. Phys.* **81**, 109 (2009).
 - ⁴ Y. Fuseya, M. Ogata, and H. Fukuyama, *Phys. Rev. Lett.* **102**, 066601 (2009) and references therein.
 - ⁵ M. Z. Hasan and C. L. Kane, *Rev. Mod. Phys.* **82**, 3045 (2010).
 - ⁶ X.-L. Qi and S.-C. Zhang, *Rev. Mod. Phys.* **83**, 1057 (2011).
 - ⁷ S.-Y. Xu, Y. Xia, L. A. Wray, S. Jia, F. Meier, J. H. Dil, J. Osterwalder, B. Slomski, A. Bansil, H. Lin, R. J. Cava, and M. Z. Hasan, *Science* **332**, 560 (2011).
 - ⁸ T. Sato, K. Segawa, K. Kosaka, S. Souma, K. Nakayama, K. Eto, T. Minami, Y. Ando, and T. Takahashi, *Nature Phys.* **7**, 840 (2011).
 - ⁹ X. Wan, A. M. Turner, A. Vishwanath, and S. Y. Savrasov, *Phys. Rev. B* **83**, 205101 (2011).
 - ¹⁰ W. Witczak-Krempa and Y. B. Kim, *Phys. Rev. B* **85**, 045124 (2012).
 - ¹¹ V. N. Kotov, B. Uchoa, V. M. Pereira, F. Guinea, and A. H. Castro Neto, *Rev. Mod. Phys.* **84**, 1067 (2012).
 - ¹² P. Goswami and S. Chakravarty, *Phys. Rev. Lett.* **107**, 196803 (2011).
 - ¹³ P. Hosur, S. A. Parameswaran, and A. Vishwanath, *Phys. Rev. Lett.* **108**, 046602 (2012).
 - ¹⁴ J. González, F. Guinea, and M. Vozmediano, *Nucl. Phys. B* **424**, 595 (1994).
 - ¹⁵ B. Roy, V. Juričić, and I. F. Herbut, *Phys. Rev. B* **87**, 041401 (2013).
 - ¹⁶ H. Isobe and N. Nagaosa, *Phys. Rev. B* **86**, 165127 (2012).
 - ¹⁷ G. S. Adkins, *Phys. Rev. D* **27**, 1814 (1983).
 - ¹⁸ P. Arnold, G. D. Moore, and L. G. Yaffe, *J. High Energy Phys.* **11**, 001 (2000).
 - ¹⁹ L. Fritz, J. Schmalian, M. Müller, and S. Sachdev, *Phys. Rev. B* **78**, 085416 (2008).
 - ²⁰ X.-L. Qi, R. Li, J. Zang, and S.-C. Zhang, *Science* **323**, 1184 (2009).